Rate Constant Calculation for HArF → Ar + HF and HKrF → Kr + HF Reactions by Dual-Level Variational Transition State Theory with Quantized Reactant State Tunneling

Yung-Lung Chen and Wei-Ping Hu*

Department of Chemistry and Biochemistry, National Chung Cheng University, Chia-Yi, Min-Hsiung, Taiwan 621

Received: January 18, 2004; In Final Form: March 12, 2004

The rate constants for the gas-phase dissociation of HArF and HKrF through the bending coordinates have been calculated using the dual-level variational transition state theory with quantized reactant state tunneling (QRST) from 20 to 600 K. Tunneling was found to dominate the reaction below 250 K, and the rate constants were found to be approximately temperature independent below 100 K. The deuterium kinetic isotope effects (KIEs) were also calculated in the same temperature range. The calculated KIEs showed dramatic increases below 250 K due to the large differences in the hydrogen and deuterium tunneling rates. Compared to the conventional tunneling method, the QRST predicts appreciably higher rate constants below 50 K and makes the transition from the temperature-dependent domain to the temperature-independent domain more sharply. At the low-temperature asymptote, the QRST predicts 30% to 40% higher KIEs than the conventional tunneling method.

Introduction

Contrary to the common chemical knowledge, the noble gases, especially xenon, show rich chemistry.[1−5] In recent years, there has been growing interest in the chemistry of lighter noble gases, which is due in large part to the preparation of various neutral noble-gas molecules in solid noble-gas matrixes.[6,7] In particular, the recent discovery of HArF,[8,9] HKrF,[10] solvated HXeOH,[11] noble-gas inserted hydrocarbons,[12−15] and various noble-gas coordinated metal complexes[16−19] showed that there are fascinating chemical bonding phenomena and reactions to be explored in this field.[20]

Although the HArF and HKrF molecules were formed and spectroscopically characterized in noble-gas matrixes, theoretical study showed that they might also be stable in the gas phase since sizable barriers exist between them and their dissociation products.[21−23] The two most important thermal dissociation pathways are to (1) the constituent atoms, H + Ng + F, and (2) the global minimum, HF + Ng (Ng = Ar, Kr). The energy barriers for these two pathways have been estimated to be ∼13 and ∼24 kcal/mol for HArF and ∼26 and ∼32 kcal/mol for HKrF.[23] The first pathways are further protected by the endoergicity of approximately 9 and 20 kcal for HArF and HKrF, respectively.[22−24] Thus, at low temperature in the gas phase, the reaction to HF + Ng, or the "bending" pathway, may become the important dissociation pathway. The bending pathways involve significant hydrogen motion, and thus large tunneling effects are expected at low temperature.

Chaban et al.[25] have estimated the tunneling rates of the HHeF → HF + He reaction using a simple WKB approximation and one-dimensional time-dependent Schrödinger equation. Large deuterium kinetic isotope effects (KIEs, ∼120) were obtained. They have also calculated the minimum energy paths of the same dissociation pathways for HArF and HKrF.[23]

Variational transition state theory (VTST)[26−28] has proved to be an invaluable tool to calculate thermal rate constants. The combination of VTST and multidimensional tunneling methods (VTST/MT)[26−31] has successfully modeled the rate constants of many different types of chemical reactions in extended temperature ranges.[32−36] For unimolecular reactions at low temperature, the reactant molecules on the reaction path are better described as residing on discrete energy levels. Thus, the tunneling effects are better modeled through these quantized energy levels instead of the continuous energy model used in most conventional semiclassical tunneling approximations.[37−39] In the current study, we applied variational transition state theory (VTST) including multidimensional tunneling (MT) at quantized reactant states to estimate the unimolecular rate constants for the dissociation of HArF and HKrF (and their deuterated analogues) through the bending coordinates. The temperature dependencies of the rate constants, tunneling effects, and the deuterium kinetic isotope effects will be calculated and discussed.

Methods

The molecular geometry and harmonic vibrational frequencies of the reactants, products, and transition states were calculated using MP2[40] and CCSD(T)[41] theory with the aug-cc-pVTZ atomic basis set.[42] Single-point energies at these stationary points were also calculated with the CCSD(T)/aug-cc-pVQZ method at the CCSD(T)/aug-cc-pVTZ geometry. The geometry, energies, gradients, and Hessians on the minimum energy paths (MEP) were calculated using the MP2/aug-cc-pVTZ method. The gradient and Hessian step sizes used in calculating the MEP were 0.005 and 0.025 bohr, respectively, on the mass-scaled coordinates with a scaling mass of 1 amu. The calculated MEP ranges are from −3.8 to 2.1 bohr for the HArF reaction, −4.5 to 2.9 bohr for the DArF reaction, −4.6 to 2.6 bohr for the HKrF reaction, and −5.5 to 3.6 bohr for the DKrF reaction. Nonredundant internal coordinates[43] were used to calculate the

* Corresponding author. E-mail: chewph@ccu.edu.tw. Fax: 886-5-272-1040.

10.1021/jp049740a CCC: $27.50
Published on Web 04/23/2004

TABLE 1: Calculated Born−Oppenheimer Energies of Reaction and Barrier Heights (in kcal/mol) for HArF → Ar + HF at Various Levels

	$\Delta V^{\ddagger}$	E_{rxn}
MP2/aug-cc-pVTZ[a]	23.0 (21.7)[b]	−134.0 (−134.2)
CCSD(T)/aug-cc-pVTZ//MP2/aug-cc-pVTZ[a]	23.7	−134.0
CCSD(T)/aug-cc-pVTZ	23.7 (22.7)	−133.9 (−133.7)
CCSD(T)/aug-cc-pVQZ//CCSD(T)/aug-cc-pVTZ	24.4	−133.5
CCSD(T)/aug-cc-pV5Z[c]		−132.1 (−131.9)
CCSD(T)/cc-pVQZ//CCSD/cc-pVTZ[d]	28.0	−137.4
B3LYP/cc-pVTZ[d]	36.1	−131.0

[a] From ref 23 and reproduced in the current study. [b] The values in parentheses are zero-point corrected values. [c] From ref 22. [d] From ref 21.

vibrational frequencies of the generalized transition states along the MEP. A dual-level[32c,44] VTST/MT dynamics calculation was performed to calculate the reaction rate constants. In the dual-level approach, the reaction-path information obtained at the MP2/aug-cc-pVTZ level (the "low-level") was corrected by the SIL-2 scheme[33a,45] based on the CCSD(T)/aug-cc-pVQZ energies and CCSD(T)/aug-cc-pVTZ geometry and frequencies on the stationary points. The barrier widths were taken directly from the MP2/aug-cc-pVTZ results. This is justified since it has been shown that the energy profiles calculated at the MP2/aug-cc-pVTZ and CCSD(T)/aug-cc-pVTZ levels are very similar.[23] Even though the barrier widths were not corrected by another intermediate-level calculation, the current dual-level approach is still different from the IOC strategies developed previously.[44] In particular, in the current approach the barrier widths (half-height widths) were controlled to that obtained from the reaction paths calculated by the MP2/aug-cc-pVTZ level after the energy corrections are made to the low-level reaction path. In the IOC methods, one has less control over the barrier widths after the energy corrections are made, and usually the corrected barrier widths would be different from that of the low-level reaction paths. The level of VTST applied is the canonical variational theory (CVT)[26,27] which locates a single reaction bottleneck at every single temperature. The tunneling correction applied was the microcanonical optimized multidimensional tunneling (μOMT)[29] method, which takes the dominant tunneling probability from the small-curvature tunneling (SCT)[30] and large-curvature tunneling (LCT)[29−31] at every energy grid point. The quantized reactant state tunneling (QRST)[38,39] scheme with the energy levels evaluated harmonically was applied. One of the degenerate bending vibrational modes at the reactant was selected as the reaction-path mode throughout the calculation. Although the nature of the reaction-path mode changes along the reaction path,[39] the current selection is justified in that the reaction path couples most strongly with the bending motion from the reactant to the TS, and the quantized energy levels are determined by the energy profile of the reaction path on the reactant side. The conventional tunneling calculation method with continuous energy levels was also applied for comparison purposes. The electronic structure calculation was performed using the Gaussian 98 program,[46] and the dual-level VTST/MT calculation was performed using the Gaussrate 8.2 program.[47]

Results and Discussion

1. HArF → Ar + HF. *1.1. Energetics and Geometry.* Table 1 shows the calculated energy barriers and energies of reaction at various theoretical levels. The barrier is estimated to be 24.4 kcal/mol at the highest level CCSD(T)/aug-cc-pVQZ//CCSD-(T)/aug-cc-pVTZ, which is also the "high-level" for energies used in the dual-level dynamics calculation. At the same level, the energy of reaction is −133.5 kcal/mol, which is close to the CCSD(T)/aug-cc-pV5Z value of −132.1 kcal/mol by Runeberg et al.[22] The MP2/aug-cc-pVTZ level, which is the "low-level" used in the dual-level dynamics calculation, gives very similar results. The calculated geometries of the stationary points at the MP2/aug-cc-pVTZ and CCSD(T)/aug-cc-pVTZ levels are depicted in Figure 1. The two levels predict very similar structures. The MP2 geometry and relative energies are identical to those obtained by Chaban et al.[23] From the reactant to the transition state (TS), the H−Ar bond is shortened by 0.078 Å, the Ar−F bond is lengthened by 0.271 Å, and the H−Ar−F bond angle changes from 180° to 106° at the CCSD(T)/aug-cc-pVTZ level. Compared to the reactant geometry obtained at the CCSD(T)/aug-cc-pV5Z level,[22] the calculated H−Ar and the Ar−F bond lengths at the CCSD(T)/aug-cc-pVTZ level are converged to within 0.01 and 0.02 Å, respectively.

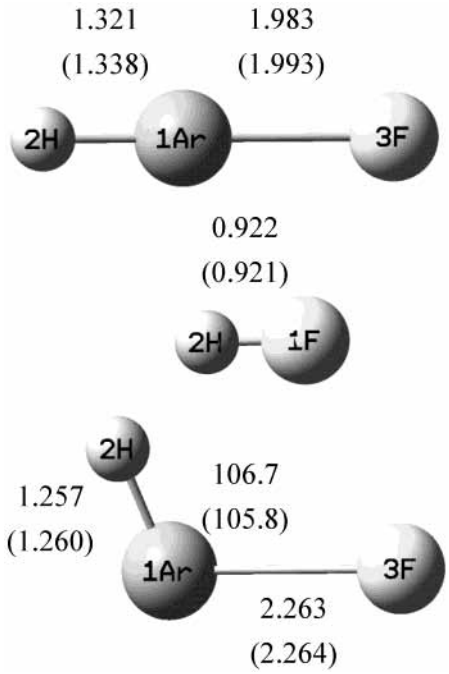

Figure 1. Calculated geometry of the reactant, product, and transition state for the HArF → Ar + HF reaction at the MP2/aug-cc-pVTZ level. The values in parentheses are the CCSD(T)/aug-cc-pVTZ results. The bond lengths are in angstroms, the angles in degrees.

1.2. Rate Constants. The calculated rate constants at a few representative temperatures from 20 to 600 K are listed in Table 2, and the Arrhenius plot is shown in Figure 2. In Table 2 we see that the variational effects (the differences between the TST and the CVT rate constants) are very small at all temperatures, as they are in most high-barrier reactions. The tunneling effects (the differences between the CVT and the CVT/μOMT rate constants) are large below 250 K and raise the rate constants dramatically at lower temperature. For example, tunneling increases the rate constants by factors of 3.0, 6.5, 1100, and 2.1×10^{18}, at 250, 200, 150, and 100 K, respectively. The SCT

TABLE 2: Calculated Rate Constants (in s^{-1}) of HArF → Ar + HF

T (K)	TST	CVT	CVT/μOMT[a]	CVT/μOMT-QRST
20	1.05 (−244)[b]	1.01 (−244)	1.37 (−22)	5.99 (−21)
27	3.82 (−178)	3.69 (−178)	2.33 (−22)	6.79 (−21)
40	2.89 (−116)	2.82 (−116)	4.91 (−22)	8.26 (−21)
50	1.60 (−90)	1.57 (−90)	7.84 (−22)	9.23 (−21)
70	4.75 (−61)	4.69 (−61)	1.79 (−21)	1.09 (−20)
100	7.10 (−39)	7.03 (−39)	6.65 (−21)	1.50 (−20)
120	3.19 (−30)	3.17 (−30)	2.34 (−20)	3.14 (−20)
150	1.53 (−21)	1.52 (−21)	1.46 (−18)	1.70 (−18)
200	8.12 (−13)	8.08 (−13)	4.39 (−12)	5.22 (−12)
250	1.49 (−7)	1.49 (−7)	3.70 (−7)	4.51 (−7)
300	5.00 (−4)	4.99 (−4)	9.00 (−4)	1.08 (−3)
400	1.33 (1)	1.33 (1)	1.82 (1)	2.07 (1)
600	3.69 (5)	3.69 (5)	4.21 (5)	4.49 (5)

[a] The conventional method using continuous energy levels for tunneling. [b] 1.05 (−244) means 1.05×10^{-244}.

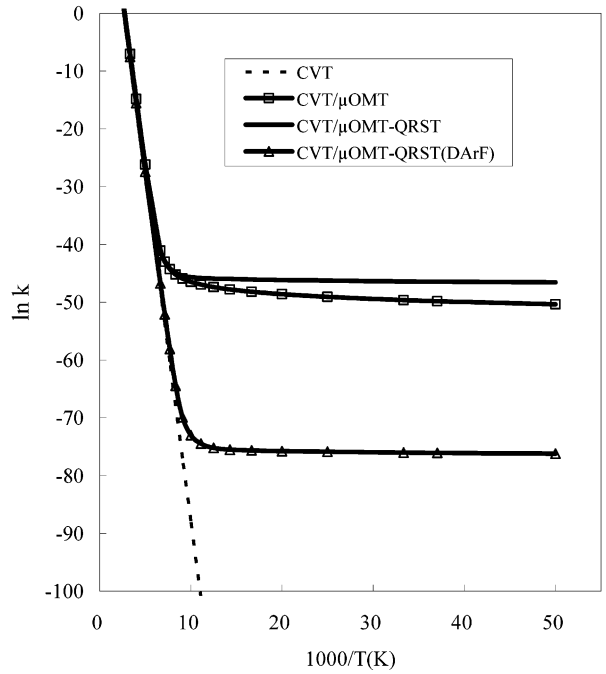

Figure 2. Arrhenius plot of the calculated rate constants for the HArF → Ar + HF reaction.

was found to be the dominant tunneling mechanism at all energies in the μOMT calculation. As seen in Table 2 and Figure 2, The CVT/μOMT-QRST rate constants become almost temperature independent below 100 K with the asymptotic value of $\sim 10^{-20}$ s^{-1}. From Figure 2, the maximum curvature of the CVT/μOMT-QRST rate constants occurs at ~125 K, which signifies the temperature at which the ground state tunneling becomes dominant.[39,48] The tunneling contribution to the low-temperature rate constants from the first four reactant states in the current QRST calculation are shown in Figure 3 together with the overall CVT/μOMT-QRST results. As seen in the figure, the ground state tunneling indeed becomes dominant at ~125 K. Compared to the conventional tunneling calculation also included in Table 2 and Figure 2, the QRST method makes the transition from the temperature-dependent domain to the temperature-independent domain more sharply and makes the asymptotic low-temperature rate constant an order of magnitude higher. This is consistent with an earlier QRST study on hydrogen atom diffusion on Cu and Ni surfaces[38,39] and on carbon tunneling in the ring expansion of 1-methylcyclobutylfluorocarbene.[48] Although both the conventional and the

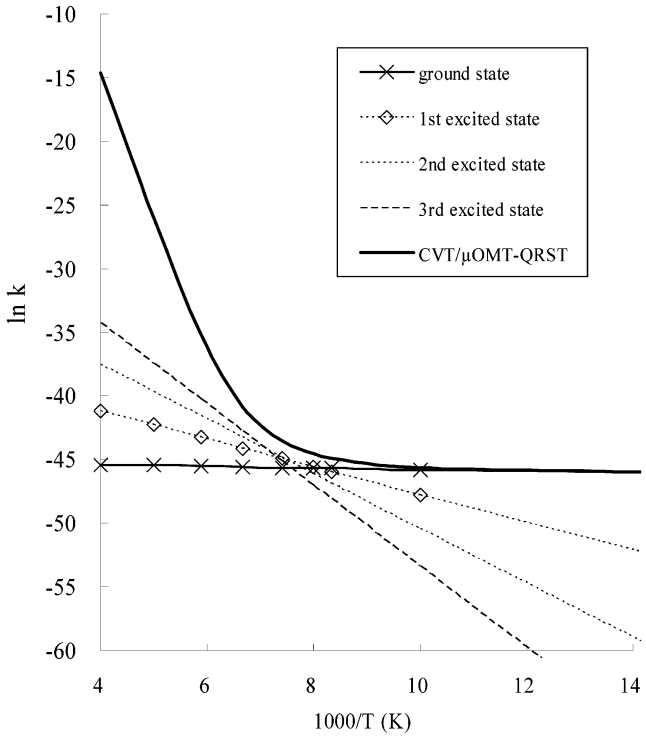

Figure 3. Arrhenius plot of the tunneling contribution from the first four reactant states to the CVT/μOMT-QRST rate constants for the HArF → Ar + HF reaction.

TABLE 3: Calculated Kinetic Isotope Effects for HArF → Ar + HF Reactions[a]

T (K)	TST	CVT	CVT/μOMT	CVT/μOMT-QRST
20	1.27 (2)[b]	1.24 (2)	5.09 (12)	7.26 (12)
27	3.36 (1)	3.31 (1)	4.96 (12)	7.25 (12)
40	9.76	9.65	4.62 (12)	7.25 (12)
50	5.84	5.79	4.24 (12)	7.24 (12)
70	3.25	3.23	3.07 (12)	6.68 (12)
100	2.09	2.08	4.20 (11)	7.62 (11)
120	1.77	1.76	2.80 (8)	3.07 (8)
150	1.50	1.49	3.15 (2)	3.42 (2)
200	1.29	1.29	3.43	4.20
250	1.20	1.20	1.94	2.56
300	1.16	1.16	1.57	2.07
400	1.14	1.14	1.33	1.67
600	1.17	1.17	1.25	1.44

[a] Kinetic isotope effect = k_H/k_D [b] 1.27 (2) means 1.27×10^2.

current methods of tunneling calculation have the same onset energy, the tunneling contribution in the conventional method is a sharply declining, continuous function of energy at very low temperature due to the Boltzmann factor, while in the QRST method the tunneling contribution is a step-function of energy with the step sizes equal to the separations of the reactant state energy levels. As a result, the calculated tunneling effects are significantly larger by the QRST method at the lowest temperature range.

1.3. Deuterium Kinetic Isotope Effects. The calculated rate constants of the deuterated reaction are also plotted in Figure 2, and the KIEs are listed in Table 3. The calculated deuterium KIE (k_H/k_D) at 300 K by TST or CVT is 1.16 which is relatively small for a reaction that involves significant hydrogen motion. This is because in the current case the reaction path corresponds to a bending mode instead of a stretching mode. In addition, this reaction has a significant inverse rotational contribution[49] ($\eta^{\ddagger}_{rot} = 0.72$) to the KIEs. The $\eta^{\ddagger}_{rot}$ is a convenient measure of

TABLE 4: Calculated Born−Oppenheimer Energies of Reaction and Barrier Heights (in kcal/mol) for HKrF → Kr + HF at Various Levels

	$\Delta V^{\ddagger}$	E_{rxn}
MP2/aug-cc-pVTZ[a]	31.4 (30.0)[b]	−112.8 (−112.7)
CCSD(T)/aug-cc-pVTZ//MP2/aug-cc-pVTZ[a]	32.1	−112.4
CCSD(T)/aug-cc-pVTZ	32.2 (30.9)	−112.4 (−112.1)
CCSD(T)/aug-cc-pVQZ//CCSD(T)/aug-cc-pVTZ	32.5	−113.1
CCSD(T)/cc-pVQZ//CCSD/cc-pVTZ[c]	34.7	−114.3
B3LYP/cc-pVTZ[c]	40.5	−110.3

[a] From ref 23 and reproduced in the current study. [b] The values in parentheses are zero-point corrected values. [c] From ref 21.

the contribution from the rotational motions of the reactant and transition state to the KIEs and is defined by

$$\eta^{\ddagger}_{rot} = \left[\frac{(\det \mathbf{I})_H^{\ddagger}\,(\det \mathbf{I})_D^{R}}{(\det \mathbf{I})_D^{\ddagger}\,(\det \mathbf{I})_H^{R}}\right]^{1/2} \quad (1)$$

where det **I** is the determinant of the moment of inertia tensor, a superscript R means reactant, a superscript ‡ means transition state, and subscripts H and D mean the hydrogenic and deuterated species, respectively. For polyatomic reaction systems this temperature-independent factor is usually larger than unity and makes an important "normal" contribution to the KIEs.[32c,32e,33a,49] However, in the current case, the $\eta^{\ddagger}_{rot}$ is less than unity and contributes to the relatively small deuterium KIEs.

The tunneling effects increase the KIE by 78% to 2.07 at 300 K. At lower temperature, the reaction is dominated by tunneling. Due to the large differences of the hydrogen and deuterium tunneling rates, the KIEs calculated by the CVT/μOMT methods become very high. For example, the KIEs calculated by the QRST method are 2.56, 4.20, 342, and 7.62 $\times$ 10^{11} at 250, 200, 150, and 100 K, respectively, while the KIEs calculated by TST or CVT, which are due mainly to the zero-point energy effects, increase at a much slower rate. The KIEs calculated by the CVT/μOMT-QRST method reach an asymptotic value of $\sim$7.3 $\times$ 10^{12} below 50 K, which is $\sim$40% higher than the CVT/μOMT value.

It is noted that in the QRST calculation, one would ideally like to use the WKB approximation[39] to obtain the energy levels in the reactant well for tunneling. However, the energy levels calculated by the WKB method are sensitive to the calculated reaction-path energies in the vicinity of the reactant well. In the direct dynamics approach[28,29,32c] (in contrast to using an analytical potential energy surface), the MEP curve in that region is usually not very reliable due to the small energy gradients. For numerical stability and reproducibility, we chose to use the harmonic method to obtain the energy levels in the current semiquantitative QRST calculation. The harmonic approximation used in the current study has the limitation that the higher energy levels are not accurately calculated since the nature of the reaction-path mode changes along the reaction path, and the energy separations are usually overestimated by the harmonic approximation. However, at the low-temperature region, which is our main focus in the current study, the dominating tunneling contribution is from the ground state where the errors introduced by the harmonic approximation were less severe.

2. HKrF → Kr + HF. *2.1. Energetics and Geometry.* Table 4 shows the calculated energy barriers and energies of reactions at various theoretical levels. The barrier is estimated to be 32.5 kcal/mol at the CCSD(T)/aug-cc-pVQZ//CCSD(T)/aug-cc-pVTZ level, which is $\sim$8 kcal/mol higher than that of the HArF reaction. At the same level, the energy of reaction is −113.1 kcal/mol, which is $\sim$20 kcal/mol higher than that of the HArF reaction. That is, the total bond energy (or the stability relative to atoms) of HKrF is 20 kcal/mol more than that of HArF. This is consistent with the energies of −7.4 and −27.8 kcal/mol for HArF and HKrF, respectively, relative to the constituent atoms calculated at the CCSD(T)/aug-cc-pVQZ//CCSD(T)/aug-cc-pVTZ level in the current study. The calculated geometries of the reactant and transition state at the MP2/aug-cc-pVTZ and CCSD(T)/aug-cc-pVTZ levels are depicted in Figure 4. Again, these two levels of theory predict very similar energies and structures. In the reactants (HNgF) of the two reactions considered here, the H−Kr bond is 0.14 Å longer than H−Ar bond while the Kr−F bond is only 0.05 Å longer than the Ar−F bond. This is consistent with earlier studies[24,50] that show that, in HNgF molecules, the H−Ng distances are much more sensitive to the identity of Ng than the Ng−F distances are. From the reactant to the TS, the H−Kr bond is shortened by 0.081 Å, the Kr−F bond is lengthened by 0.289 Å, and the H−Kr−F bond angle changes from 180° to 102° at the CCSD(T)/aug-cc-pVTZ level. Compared to the HArF reaction, the changes in bond lengths are very similar, and in the TS the H−Kr−F angle is 4° smaller than the H−Ar−F angle.

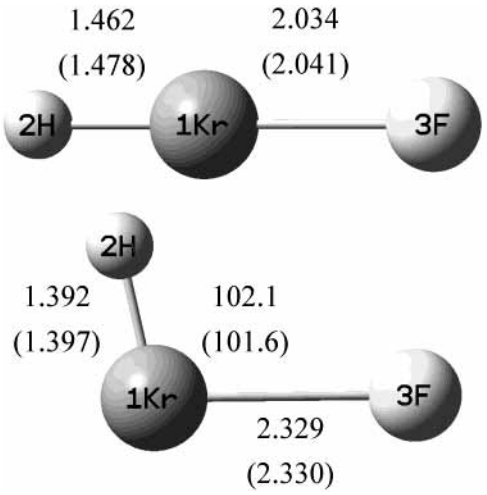

Figure 4. Calculated geometry of the reactant and transition state for the HKrF → Kr + HF reaction at the MP2/aug-cc-pVTZ level. The values in parentheses are the CCSD(T)/aug-cc-pVTZ results. The bond lengths are in angstroms, the angles in degrees.

2.2. Rate Constants. The calculated rate constants at a few representative temperatures from 20 to 600 K are listed in Table 5, and the Arrhenius plot is shown in Figure 5. Due to the higher barrier, the calculated rate constant at 300 K is approximately 6 orders of magnitude lower than that of the HArF reaction. As seen in Table 5, the variational effects are very small except at the lowest temperatures, and tunneling dominates the reaction below 250 K, which is very similar to the HArF reaction. The tunneling increases the rate constants by factors of 1.9, 4.2, 134, and 2.5 $\times$ 10^{20}, at 250, 200, 150, and 100 K, respectively. The SCT was found to be the dominant tunneling mechanism at all

TABLE 5: Calculated Rate Constants (s^{-1}) of HKrF → Kr + HF

T (K)	TST	CVT	CVT/μOMT[a]	CVT/μOMT-QRST
20	8.98 (−314)[b]	8.05 (−314)	1.23 (−37)	4.55 (−36)
27	2.35 (−241)	2.15 (−241)	2.28 (−37)	4.95 (−36)
40	6.52 (−159)	6.16 (−159)	5.60 (−37)	5.69 (−36)
50	1.26 (−124)	1.20 (−124)	1.12 (−36)	6.20 (−36)
70	2.17 (−85)	2.10 (−85)	4.63 (−36)	7.22 (−36)
100	6.81 (−56)	6.65 (−56)	3.24 (−35)	1.65 (−35)
120	2.16 (−44)	2.12 (−44)	1.99 (−34)	1.19 (−34)
150	7.33 (−33)	7.21 (−33)	7.71 (−31)	9.64 (−31)
200	2.75 (−21)	2.71 (−21)	1.21 (−20)	1.14 (−20)
250	2.59 (−14)	2.56 (−14)	6.00 (−14)	4.92 (−14)
300	1.19 (−9)	1.19 (−9)	2.08 (−9)	1.62 (−9)
400	8.45 (−4)	8.40 (−4)	1.14 (−3)	8.89 (−4)
600	6.17 (2)	6.15 (2)	7.01 (2)	5.84 (2)

[a] The conventional method using continuous energy levels for tunneling. [b] 8.98 (−314) means 8.98×10^{-314}.

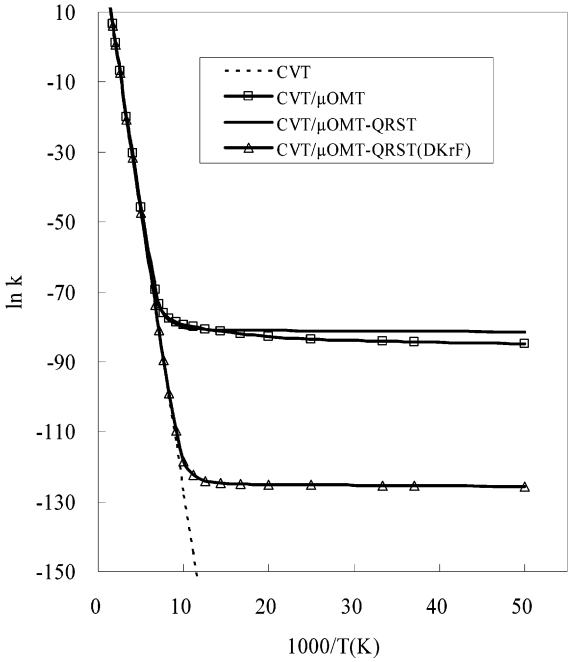

Figure 5. Arrhenius plot of the calculated rate constants for the HKrF → Kr + HF reaction.

energies in the μOMT calculation. As seen in Table 5 and Figure 5, The CVT/μOMT-QRST rate constants become almost temperature independent below 70 K with the asymptotic value $\sim 10^{-35}$ s^{-1}, which is approximately 15 orders of magnitude lower than that of the HArF reaction. Figure 5 shows that the maximum curvature of the CVT/μOMT-QRST rate constants occurs at ~125 K, also similar to the HArF reaction.

2.3. Deuterium Kinetic Isotope Effects. The calculated rate constants of the deuterated reaction are also plotted in Figure 5, and the KIEs are listed in Table 6. The calculated deuterium KIE at 300 K by TST or CVT is 1.36, and the tunneling effects increase the KIE by 33% to 1.81. At lower temperature, the reaction is dominated by tunneling, and the KIEs calculated by the CVT/μOMT methods become very high. For example, the KIEs calculated by the QRST method are 2.46, 4.73, 92.9, and 4.76×10^{16} at 250, 200, 150, and 100 K, respectively, and reach an asymptotic value of $\sim 1.5 \times 10^{19}$ below 50 K, which is ~30% higher than the CVT/μOMT value. This value is approximately 6 orders of magnitude higher than that of the HArF reaction.

3. Thermal Stability of HArF and HKrF. Experimental evidence shows that HArF and HKrF molecules in the stable sites of noble-gas matrixes are stable up to 40 K, while thermal

TABLE 6: Calculated Kinetic Isotope Effects for HKrF → Kr + HF Reactions[a]

T (K)	TST	CVT	CVT/μOMT	CVT/μOMT-QRST
20	2.74 (3)[b]	2.47 (3)	1.22 (19)	1.58 (19)
27	2.11 (2)	1.94 (2)	1.24 (19)	1.49 (19)
40	3.35 (1)	3.17 (1)	1.30 (19)	1.41 (19)
50	1.56 (1)	1.50 (1)	1.45 (19)	1.37 (19)
70	6.53	6.33	1.63 (19)	1.12 (19)
100	3.40	3.32	1.81 (17)	4.76 (16)
120	2.64	2.59	2.34 (9)	1.21 (9)
150	2.07	2.03	6.94 (1)	9.29 (1)
200	1.64	1.62	4.11	4.73
250	1.46	1.45	2.40	2.46
300	1.37	1.36	1.89	1.81
400	1.29	1.29	1.53	1.42
600	1.28	1.27	1.37	1.28

[a] Kinetic isotope effect = k_H/k_D. [b] 2.74 (3) means 2.74×10^3.

decomposition is observed at 27−32 K for molecules in unstable sites.[9,10] The decomposition in the matrixes has been attributed to reactions with reactive radicals[8−10] since the rates of the two unimolecular decomposition pathways mentioned in the Introduction should be extremely low at these temperatures, and no significant deuterium isotope effects on the decomposition have been experimentally identified.[10] For example, the rate constant of HArF → Ar + HF at 30 K was calculated to be only 7×10^{-21} s^{-1} in the current study. If pure HArF or HKrF can be made in the gas phase, they should be thermally stable. For example, at 100 K, the decomposition rate constants through the bending coordinates are calculated to be only 1.50×10^{-20} and 1.65×10^{-35} s^{-1} for HArF and HKrF, respectively. While the tunneling effects increase the rate constants tremendously at low temperature, the increases are less dramatic above 200 K. For example, the CVT/μOMT-QRST rate constants for HArF are factors of 6 and 2 larger than the CVT values at 200 and 300 K, respectively. Thus at higher temperature, dissociation to the constituent atoms might be more important due to the lower energy barriers. The dual-level VTST/MT rate constant calculation on the decomposition of HArF and HKrF to the constituent atoms is currently in progress in our laboratory.

Summary

We have performed a dual-level variational transition state theory with multidimensional tunneling calculation on the dissociation reactions HArF → Ar + HF, HKrF → Kr + HF, and their deuterated analogues from 20 to 600 K with the quantized reactant state tunneling method. The tunneling effects were found to dominate the reactions below 250 K and become extremely important at lower temperature. The calculation predicted that the rate constants begin to level off at approximately 100 K and become temperature independent at even lower temperature. The kinetic isotope effects were modest at room temperature (KIEs are ~2 at 300 K) and increase rapidly as the temperature decreases. Compared to the conventional tunneling methods, the QRST method predicts sharper transitions from the temperature-dependent domains to the temperature-independent domains, higher asymptotic rate constants, and larger asymptotic deuterium isotope effects.

Acknowledgment. This work is supported in part by the National Science Council of Taiwan, Grant No. NSC 92-2113-M194-019. We thank Professor Truhlar of the University of Minnesota for providing the Gaussrate interface program. We are also grateful to the National Center for High-Performance Computing of Taiwan for providing part of the computational resources.

References and Notes

(1) Bartlett, N. *Proc. Chem. Soc.* **1962**, 218.

(2) Hawkins, D. T.; Falconer, W. E.; Bartlett, N. *Noble-Gas Compounds. A Bibliography*: *1962*−*1976*; IFI/Plenum: New York, 1978.

(3) Cotton, F. A.; Wilkinson, G. *Advanced Inorganic Chemistry*; Wiley: New York, 1980.

(4) Holloway, J. H.; Schrobilgen, G. J. *Inorg. Chem.* **1981**, *20*, 3363.

(5) Laszlo, P.; Schrobilgen, G. J. *Angew. Chem., Int. Ed. Engl.* **1988**, *27*, 479.

(6) Pettersson, M.; Lundell, J.; Räsänen, M. *J. Chem. Phys.* **1995**, *102*, 6423.

(7) Pettersson, M.; Lundell, J.; Räsänen, M. *J. Chem. Phys.* **1995**, *103*, 205.

(8) Khriachtchev, L.; Pettersson, M.; Runeberg, N.; Lundell, J.; Räsänen, M. *Nature* **2000**, *406*, 874.

(9) Khriachtchev, L.; Pettersson, M.; Lignell, A.; Räsänen, M. *J. Am. Chem. Soc.* **2001**, *123*, 8610.

(10) Pettersson, M.; Khriachtchev, L.; Lignell, A.; Räsänen, M. *J. Chem. Phys.* **2002**, *116*, 2508.

(11) Nemukhin, A. V.; Grigorenko, B. L.; Khriachtchev, L.; Tanskanen, H.; Pettersson, M.; Räsänen, M. *J. Am. Chem. Soc.* **2002**, *124*, 10706.

(12) Tanskanen, H.; Khriachtchev, L.; Lundell, J.; Kiljunen, H.; Räsänen, M. *J. Am. Chem. Soc.* **2003**, *125*, 16361.

(13) Khriachtchev, L.; Tanskanen, H.; Lundell, J.; Pettersson, M.; Kiljunen, H.; Räsänen, M. *J. Am. Chem. Soc.* **2003**, *125*, 4696.

(14) Feldman, V. I.; Sukhov, F. F.; Orlov, A. Y.; Tyulpina, I. V. *J. Am. Chem. Soc.* **2003**, *125*, 4698.

(15) Khriachtchev, L.; Tanskanen, H.; Cohen, A.; Gerber, R. B.; Lundell, J.; Pettersson, M.; Kiljunen, H.; Räsänen, M. *J. Am. Chem. Soc.* **2003**, *125*, 6876.

(16) Seidel, S.; Seppelt, K. *Science* **2000**, *290*, 117.

(17) Drews, T.; Seidel, S.; Seppelt, K. *Angew. Chem., Int. Ed.* **2002**, *41*, 454.

(18) Li, J.; Bursten, B. E.; Liang, B.; Andrews, L. *Science* **2002**, *295*, 2242.

(19) Andrews, L.; Liang, B.; Li, J.; Bursten, B. E. *J. Am. Chem. Soc.* **2003**, *125*, 3126.

(20) Christe, K. O. *Angew. Chem., Int. Ed.* **2001**, *40*, 1419.

(21) Wong, M. W. *J. Am. Chem. Soc.* **2000**, *122*, 6289.

(22) Runeberg, N.; Pettersson, M.; Khriachtchev, L.; Lundell, J.; Räsänen, M. *J. Chem. Phys.* **2001**, *114*, 836.

(23) Chaban, G. M.; Lundell, J.; Gerber, R. B. *Chem. Phys. Lett.* **2002**, *364*, 628.

(24) Lundell, J.; Chaban, G. M.; Gerber, R. B. *Chem. Phys. Lett.* **2000**, *331*, 308.

(25) Chaban, G. M.; Lundell, J.; Gerber, R. B. *J. Chem. Phys.* **2001**, *115*, 7341.

(26) Truhlar, D. G.; Garrett, B. C. *Acc. Chem. Res.* **1980**, *13*, 440.

(27) Truhlar, D. G.; Isaacson, A. D.; Garrett, B. C. In *Theory of Chemical Reaction Dynamics*; Baer, M., Ed.; CRC Press: Boca Raton, FL, 1985; Vol. 4, p 65.

(28) Truhlar, D. G.; Garrett, B. C.; Klippenstein, S. J. *J. Phys. Chem.* **1996**, *100*, 12771.

(29) Liu, Y.-P.; Lu, D.-H.; Gonzalez-Lafont, A.; Truhlar, D. G. *J. Am. Chem. Soc.* **1993**, *115*, 7806.

(30) (a) Liu, Y.-P.; Lynch, G. C.; Truong, T. N.; Lu, D.-H.; Truhlar, D. G.; Garrett, B. C. *J. Am. Chem. Soc.* **1993**, *115*, 2408. (b) Lu, D.-H.; Truong, T. N.; Melissas, V. S.; Lynch, G. C.; Liu, Y.-P.; Garrett, B. C.; Steckler, R.; Isaacson, A. D.; Rai, S. N.; Hancock, G. C.; Lauderdale, J. G.; Joseph, T.; Truhlar, D. G. *Comput. Phys. Commun.* **1992**, *71*, 235.

(31) Truong, T. N.; Lu, D.-H.; Lynch, G. C.; Liu, Y.-P.; Melissas, V. S.; Gonzalez-Lafont, A.; Rai, S. N.; Steckler, R.; Garrett, B. C.; Joseph, T.; Truhlar, D. G. *Comput. Phys. Commun.* **1993**, *75*, 143.

(32) (a) Melissas, V. S.; Truhlar, D. G. *J. Chem. Phys.* **1993**, *99*, 1013. (b) Melissas, V. S.; Truhlar, D. G. *J. Phys. Chem.* **1994**, *98*, 875. (c) Corchado, J. C.; Espinosa-Garcia, J.; Hu, W.-P.; Rossi, I.; Truhlar, D. G. *J. Phys. Chem.* **1995**, *99*, 687. (d) Hu, W.-P.; Rossi, I.; Corchado, J. C.; Truhlar, D. G. *J. Phys. Chem. A* **1997**, *101*, 6911. (e) Lien, P.-Y.; You, R.-M.; Hu, W.-P. *J. Phys. Chem. A* **2001**, *105*, 2391.

(33) (a) Huang, C.-H.; Tsai, L.-C.; Hu, W.-P. *J. Phys. Chem. A* **2001**, *105*, 9945. (b) Fu, Y.-S.; Tsai, S.-C.; Huang, C.-H.; Yen, S.-Y.; Hu, W.-P.; Yu, S. J. *J. Org. Chem.* **2003**, *68*, 3068.

(34) (a) Gonzalez-Lafont, A.; Lluch, J. M.; Espinosa-Garcia, J. *J. Phys. Chem. A* **2001**, *105*, 10553. (b) Espinosa-Garcia, J. *J. Phys. Chem. A* **2002**, *106*, 5686. (c) Espinosa-Garcia, J. *J. Phys. Chem. A* **2003**, *107*, 1618.

(35) (a) Masgrau, L.; Gonzalez-Lafont, A.; Lluch, J. M. *J. Chem. Phys.* **2001**, *114*, 2154. (b) Masgrau, L.; Gonzalez-Lafont, A.; Lluch, J. M. *J. Phys. Chem. A* **2002**, *106*, 11760. (c) Masgrau, L.; Gonzalez-Lafont, A.; Lluch, J. M. *J. Phys. Chem. A* **2003,** *107*, 4490.

(36) (a) Nicoll, R. M.; Hillier, I. H.; Truhlar, D. G. *J. Am. Chem. Soc.* **2001**, *123*, 1459. (b) Skokov, S.; Zou, S.; Bowman, J. M.; Allison, T. C.; Truhlar, D. G.; Lin, Y.; Ramachandran, B.; Garrett, B. C.; Lynch, B. J. *J. Phys. Chem. A* **2001**, *105*, 2298. (c) McRae, R. P.; Schenter, G. K.; Garrett, B. C.; Svetlicic, Z.; Truhlar, D. G. *J. Chem. Phys.* **2001**, *115*, 8460. (d) Pu, J.; Corchado, J. C.; Truhlar, D. G. *J. Chem. Phys.* **2001**, *115*, 6266. (e) Truhlar, D. G.; Gao, J.; Alhambra, C.; Garcia-Viloca, M.; Corchado, J.; Sánchez, M. L.; Villà, J. *Acc. Chem. Res.* **2002**, *35*, 341. (f) Pu, J.; Truhlar, D. G. *J. Chem. Phys.* **2002**, *117*, 1479. (g) Albu, T. V.; Lynch, B. J.; Truhlar, D. G.; Goren, A. C.; Hrovat, D. A.; Borden, W. T.; Moss, R. A. *J. Phys. Chem. A* **2002**, *106*, 5323.

(37) Lauderdale, J. G.; Truhlar, D. G. *Surf. Sci.* **1985**, *164*, 558.

(38) Wonchoba, S. E.; Hu, W.-P.; Truhlar, D. G. In *Theoretical and Computational Approaches to Interface Phenomena*; Sellers, H. L., Golab, J. T., Eds.; Plenum Press: New York, 1994; p 1.

(39) Wonchoba, S. E.; Hu, W.-P.; Truhlar, D. G. *Phys. Rev. B* **1995**, *51*, 9985.

(40) Møller, C.; Plesset, M. S. *Phys. Rev.* **1934**, *46*, 618.

(41) Raghavachari, K.; Trucks, G. W.; Pople, J. A.; Head-Gordon, M. *Chem. Phys. Lett.* **1989**, *157*, 479.

(42) (a) Dunning, T. H., Jr. *J. Chem. Phys.* **1989**, *90*, 1007. (b) Kendall, R. A.; Dunning, T. H., Jr.; Harrison, R. J. *J. Chem. Phys.* **1992**, *96*, 6769. (c) Woon, D. E.; Dunning, T. H., Jr. *J. Chem. Phys.* **1993**, *98*, 1358. (d) Wilson, A. K.; Woon, D. E.; Peterson, K.; Dunning, T. H., Jr. *J. Chem. Phys.* **1999**, *110*, 7667.

(43) Jackel, C. F.; Gu, Z.; Truhlar, D. G. *J. Chem. Phys.* **1995**, *102*, 3188.

(44) Hu, W.-P.; Liu, Y.-P.; Truhlar, D. G. *J. Chem. Soc., Faraday Trans.* **1994**, *90*, 1715.

(45) Huang, C.-H.; You, R.-M.; Lian, P.-Y.; Hu, W.-P. *J. Phys. Chem. A* **2000**, *104*, 7200.

(46) Frisch, J. M.; Trucks, W. G.; Schlegel, B. H.; Scuseria, E. G.; Robb, A. M.; Cheeseman, R. J.; Zakrzewski, G. V.; Montgomery, A. J., Jr.; Stratmann, E. R.; Burant, C. J.; Dapprich, S.; Millam, M. J.; Daniels, D. A.; Kudin, N. K.; Strain, C. M.; Farkas, O.; Tomasi, J.; Barone, V.; Cossi, M.; Cammi, R.; Mennucci, B.; Pomelli, C.; Adamo, C.; Clifford, S.; Ochterski, J.; Petersson, A. G.; Ayala, Y. P.; Cui, Q.; Morokuma, K.; Rega, N.; Salvador, P.; Dannenberg, J. J.; Malick, K. D.; Rabuck, D. A.; Raghavachari, K.; Foresman, B. J.; Cioslowski, J.; Ortiz, V. J.; Baboul, G. A.; Stefanov, B. B.; Liu, G.; Liashenko, A.; Piskorz, P.; Komaromi, I.; Gomperts, R.; Martin, L. R.; Fox, J. D.; Keith, T.; Al-Laham, A. M.; Peng, Y. C.; Nanayakkara, A.; Challacombe, M.; Gill, W. M. P.; Johnson, B.; Chen, W.; Wong, W. M.; Andres, L. J.; Gonzalez, C.; Head-Gordon, M.; Replogle, S. E.; Pople, A. J. *Gaussian 98*, revision A.11.3; Gaussian, Inc.: Pittsburgh, PA, 2002.

(47) Corchado, J. C.; Chunag, Y.-Y.; Coitino, E. L.; Truhlar, D. G. *Gaussrate*, version 8.2; University of Minnesota: Minneapolis, MN, 1999.

(48) Zuev, P. S.; Sheridan, R. S.; Albu, T. V.; Truhlar, D. G.; Hrovat, D. A. *Science* **2003**, *299*, 867.

(49) (a) Hu, W.-P.; Truhlar, D. G. *J. Am. Chem. Soc.* **1996**, *118*, 860. (b) Hu, W.-P.; Truhlar, D. G. *J. Am. Chem. Soc.* **1995**, *117*, 10726. (c) Hu, W.-P.; Truhlar, D. G. *J. Am. Chem. Soc.* **1994**, *116*, 7800.

(50) Yen, S.-Y.; Mou, C.-H.; Hu, W.-P. *Chem. Phys. Lett.* **2004**, *383*, 606.